ResearchGate

See discussions, stats, and author profiles for this publication at: https://www.researchgate.net/publication/49843804

High Frequency Vibrational Modulations in Two-Dimensional Electronic Spectra and Their Resemblance to Electronic Coherence Signatures

ARTICLE *in* THE JOURNAL OF PHYSICAL CHEMISTRY B · FEBRUARY 2011

Impact Factor: 3.3 · DOI: 10.1021/jp109442b · Source: PubMed

CITATIONS
74

READS
68

7 AUTHORS, INCLUDING:

Franz Milota
JTI R&D
51 PUBLICATIONS **902** CITATIONS
SEE PROFILE

Jürgen Hauer
TU Wien
51 PUBLICATIONS **800** CITATIONS
SEE PROFILE

Jaroslaw Sperling
University of Vienna
35 PUBLICATIONS **675** CITATIONS
SEE PROFILE

Oliver Bixner
Nanyang Technological University
6 PUBLICATIONS **192** CITATIONS
SEE PROFILE

Available from: Oliver Bixner
Retrieved on: 26 January 2016

THE JOURNAL OF PHYSICAL CHEMISTRY B

ARTICLE

pubs.acs.org/JPCB

High Frequency Vibrational Modulations in Two-Dimensional Electronic Spectra and Their Resemblance to Electronic Coherence Signatures

N. Christensson,[†] F. Milota,[‡] J. Hauer,[†] J. Sperling,[†] O. Bixner,[†] A. Nemeth,[†] and H. F. Kauffmann[*,†,§]

[†]Electronic Properties of Materials, Faculty of Physics, University of Vienna, Strudlhofgasse 4, 1090 Vienna, Austria

[‡]Lehrstuhl für BioMolekulare Optik, Ludwig-Maximilians-University, Oettingenstrasse 67, 80538 Munich, Germany

[§]Ultrafast Dynamics Group, Faculty of Physics, Vienna University of Technology, Wiedner Hauptstrasse 8-10, 1040 Vienna, Austria

ABSTRACT: In this work we analyze how nuclear coherences modulate diagonal and off-diagonal peaks in two-dimensional electronic spectroscopy. 2D electronic spectra of pinacyanol chloride are measured with 8 fs pulses, which allows coherent excitation of the 1300 cm^{-1} vibrational mode. The 2D spectrum reveals both diagonal and off-diagonal peaks related to the vibrational mode. On early time scales, up to 30 fs, coherent dynamics give rise to oscillations in the amplitudes, positions, and shapes of the peaks in the 2D spectrum. We find an anticorrelation between the amplitude and the diagonal width of the two diagonal peaks. The measured data are reproduced with a model incorporating a high frequency mode coupled to an electronic two-level-system. Our results show that these anticorrelated oscillations occur for vibrational wavepackets and not exclusively for electronic coherences as has been assumed previously.

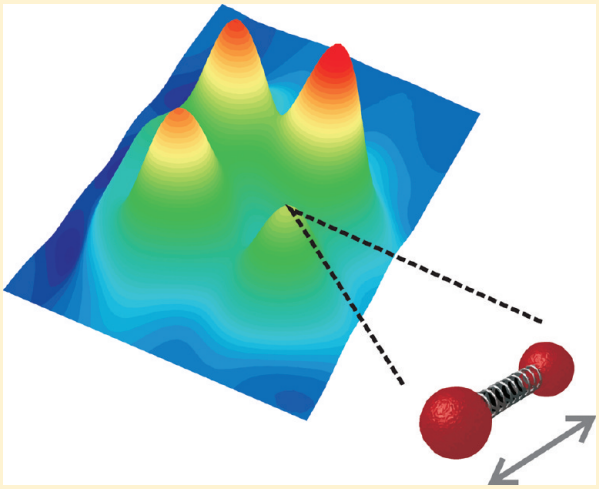

INTRODUCTION

Generation of wavepackets, i.e., the coherent superposition of multiple quantum states,[1] is a concept at the very heart of quantum mechanics. With their large spectral bandwidth, ultrashort optical pulses readily excite nuclear wavepackets consisting of vibrational modes up to several thousand wavenumbers.[2−7] Time resolved measurements map out the potential energy surface (PES) of the modes coupling to the electronic transition and elucidate coupling to dark modes via relaxation and dephasing processes.[8] Besides coherent excitation of vibrational states, a superposition of electronic states is also possible. Intermolecular electronic coherences are of great interest to the field of energy transfer in pigment−protein complexes[9−12] and tubular nanostructures.[13,14] Experiments have shown that electronic coherences in protein−pigment complexes survive for more than 100 fs at room temperature[15] and substantially longer at cryogenic temperatures.[16,17] Given such long lifetimes, the exciton can irreversibly sample the aggregate energy landscape and thereby increase the energy transfer efficiency. Recently, a number of experiments have indicated that long-lived electronic coherences may be a general feature of excitonic systems.[18−20]

While electronic coherence in such systems is a collective excitonic effect involving many pigments, nuclear coherence is concerned with modes localized on a single chromophore. The later coherence is an inherent feature of all pigments and cannot be neglected in studies of pigment complexes with delocalized electronic states. At this point one may ask how to distinguish between electronic and nuclear coherence in an experiment.[21] The left-hand side of Figure 1 shows the energy level structure of an electronic two-level system (TLS) coupled to a single vibrational mode on each state. The right side of Figure 1 shows the excitonic energy levels of two coupled electronic TLSs. While there are some differences, like the doubly excited state f in the dimer or the ground state vibrational mode in the monomeric system, most of the Liouville pathways that can be constructed for the two energy level schemes are identical. More specifically, both models of single-exciton and electronic-vibrational level schemes (cf. Figue 1) result in the same Liouville pathways for the single-exciton manifold. In spite of these similarities, there are a few pathways unique to each model. However, facing obstacles like limited spectral bandwidth, strong system−bath interaction, or a complex energy level structure,

Special Issue: Shaul Mukamel Festschrift

Received: October 1, 2010
Revised: January 14, 2011
Published: February 17, 2011

ACS Publications © 2011 American Chemical Society

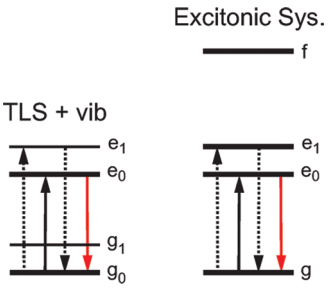

Figure 1. (Left side) Energy level structure of an electronic two-level system coupled to a single vibrational mode with a low Huang−Rhys factor. The vibrational mode is present in both the ground and excited state. Dashed (full) arrows stand for ket (bra) interactions while the colored arrows represent the emerging signal field. (right side) The energy level structure of an excitonic dimer formed by resonant coupling of two electronic two-level systems. The coupling splits the first excited state and gives rise to a doubly excited state, f, formed by simultaneous excitation of both monomers. The four arrows in each figure illustrate one specific Liouville pathway common to both systems that would be indistinguishable experimentally.

it is far from obvious if these features can be detected unambiguously.

The study of coherences (nuclear or electronic) is facilitated greatly by experimental techniques isolating them from population contributions. For this purpose, two-dimensional electronic spectroscopy (2D-ES)[22−24] is an ideal tool because coherences give rise to off-diagonal peaks in two-dimensional spectra. Besides static off-diagonal peaks, oscillating coherence pathways will contribute to the signals and modulate the diagonal and off-diagonal peaks. While the observation of static off-diagonal peaks[25] does not clarify the nature of the coherence (cf. Figure 1), it is widely accepted that an anticorrelation between the width and the amplitude of a peak (both diagonal and off-diagonal) is indicative of electronic coherence.[16,18] This argument is based on a simulation study of an excitonic dimer.[26] However, it is not clear (and was not dealt with so far) if this type of modulation is unique to electronic coherences or if a similar pattern may also arise from nuclear coherences. In the following we address this issue by recording time-resolved 2D electronic spectra of a cyanine dye in solution. This monomeric system can only show nuclear coherences. By recording the 2D spectra with 8 fs pulses we resolve multiple diagonal and off-diagonal peaks due to a high frequency vibrational (nuclear) mode. Following the waiting time (t_2) dependence of the 2D spectra, resolves the oscillatory change of both the overall signal pattern and the individual peaks.

METHODS

Experimental Section. A titanium-sapphire amplifier with a repetition rate of 200 kHz (RegA 9050, Coherent Inc.) pumps a noncollinear optical parametric amplifier (NOPA).[27] The pulses are compressed with a combination of Brewster-angle chirped mirrors and a pair of fused silica prisms.[28] This yields nearly Fourier limited 7.8 fs pulses with a bandwidth of 1900 cm^{-1}, corresponding to a time-bandwidth product of 0.45. Figure 2a shows the second harmonic generation frequency resolved optical gating (SHG-FROG) trace[29] of the pulses recorded at

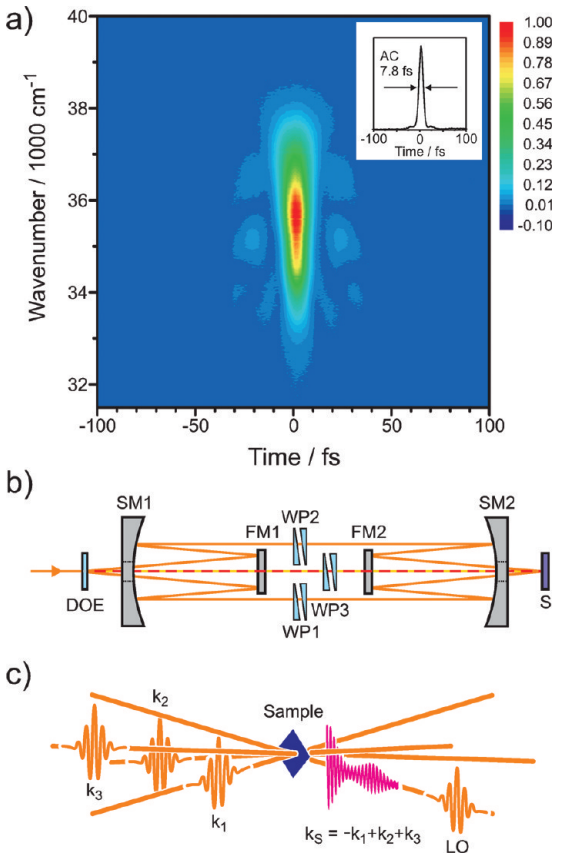

Figure 2. (a) Frequency resolved optical gating trace of the pulses with a duration of 7.8 fs. The inset shows the frequency integrated autocorrelation. (b) Schematic of the experimental setup: DOE is the diffractive optical element; SM is the spherical mirror; FM is the folding mirror; WP is the wedge pair; S is the sample. (c) Definition of the pulse sequence.

the sample position with a 10 μm thick β-bariumborate (BBO) crystal.

2D-ES is a four-wave mixing technique which correlates transition dipole moment fluctuations during different time periods. In this experiment a sequence of three laser pulses with wave vectors $-\mathbf{k_1}$, $\mathbf{k_2}$, and $\mathbf{k_3}$ excites the sample and generates a third order polarization $P_S^{(3)}(k_S;t_1;t_2;t_3)$, which emits a signal field in the $\mathbf{k_S} = -\mathbf{k_1} + \mathbf{k_2} + \mathbf{k_3}$ phase-matching direction. We denote t_1 (t_2) as the delay between the first and second pulse (second and third pulse) arriving at the sample, while t_3 stands for the temporal separation between the last pulse and the signal field. The radiated signal field is characterized in amplitude and phase via spectral interferometry with the local oscillator (LO). Different signal contributions are measured depending on the order in which the pulses interact with the sample. With the pulse along the direction of $-\mathbf{k_1}$ ($\mathbf{k_2}$) arriving first at the sample we collect rephasing (R) (nonrephasing (NR)) signals by scanning the delay t_1 from 0 to 100 fs. Summation of R and NR contributions leads to absorptive real part and dispersive imaginary part spectra.[30]

Figure 2b shows a scheme of the experimental 2D-ES setup. Fourier transformation in the evaluation of the experimental data requires high accuracy and stability of the relevant time delays. This is achieved by a passively phase-stabilized setup for the generation of the three excitation pulses and the LO.[31,32] Briefly,

a diffractive optical element splits the beam into four beams of equal intensity, arranged in a tilted folded boxcar geometry.[33] The four beams pass through a hole in the middle of the first spherical mirror (SM1) and are reflected by the first folding mirror (FM1) back onto SM1. These parallelized beams pass FM1 at the top, bottom, left, and right side. The three excitation beams pass identical glass wedge pairs (WP1−3), mounted on computer controlled linear delay stages, to introduce time delays with a resolution of 5.3 attoseconds.[31] The beam at the top is the LO, which precedes the excitation beams by ≈540 fs, and can be attenuated with a variable neutral density filter by up to 4 orders of magnitude. After the delay stages, an identical arrangement of folding (FM2) and spherical mirror (SM2) focuses all four beams to a common spot with a diameter of 200 μm. The third order signal propagates collinearly with the LO. Both are spatially filtered from the excitation pulses and detected with a photodiode array to obtain the ω_3 frequency axis. The absolute phases of the 2D spectra were determined for each t_2 value by phasing to the spectrally resolved pump−probe signal according to the projection slice theorem.[23,34]

Pinacyanol chloride (1,1′-diethyl-2,2′-carbocyanine chloride, PIN) was purchased from Sigma Aldrich and used as received. Solutions with $c = 1.25 \times 10^{-4}$ M were prepared in spectrophotometric grade methanol giving an optical density of 0.25 at the central laser frequency. Figure 3a shows the absorption spectrum (solid black line) with the pulse spectrum (gray shaded area). PIN exhibits three well resolved peaks at 16 580, 17 860, and 19 200 cm^{-1}. On the basis of a DFT analysis with a B3LYP functional,[35] we find that this mode is best described by in-plane wagging motion of the aromatic rings of the molecule. The 1300 cm^{-1} mode leads to a modulation of the third order signals with a period of 25 fs (cf. Figure 3b and c). The central excitation frequency of our laser pulses was tuned to 18 020 cm^{-1}, covering the first and second peak in the vibrational progression. We used a wire-guided flow jet for sample handling,[36,37] where a micro-gear pump circulates the solution at a rate of ∼20 mL/s. Under the employed excitation conditions, i.e., energy of 4 nJ per pulse and a film thickness of ≈200 μm, this results in excitation of 1.6% of the molecules in the sample volume, or a fluence of 1.3×10^{14} photons/cm^2, respectively.

Theory. Using third order perturbation theory, we can express the induced nonlinear polarization via the (third order) response functions convoluted with the electric fields[34]

$$P(k_s, t_3) = \int_0^\infty d\tau_1 \int_0^\infty d\tau_2 \int_0^\infty d\tau_3\, S^{(3)}(\tau_1, \tau_2, \tau_3) \cdot E(t_3 - \tau_1 - \tau_2 - \tau_3) E(t_3 - \tau_2 - \tau_3) E(t_3 - \tau_3) \quad (1)$$

Here, $S^{(3)}$ is the third order response function and E are the electric fields. τ_1 and τ_2 denote the time delay between first and second- and second and third-interaction with the respective electric fields, while τ_3 denotes the delay between the last interaction and the signal field. Integration over τ_i emphasizes the use of pulses with finite duration rather than δ-pulses.

The response functions contain all relevant information on the system and its dynamics. The form of the response functions depend on the electronic structure of the system under study. In this work we restrict our analysis to an electronic two-level system. Contributions from nuclear degrees of freedom are considered in the line shape function $g(t)$ as discussed below. For this case, only four unique response functions need to be considered, namely the ground and excited state rephasing and

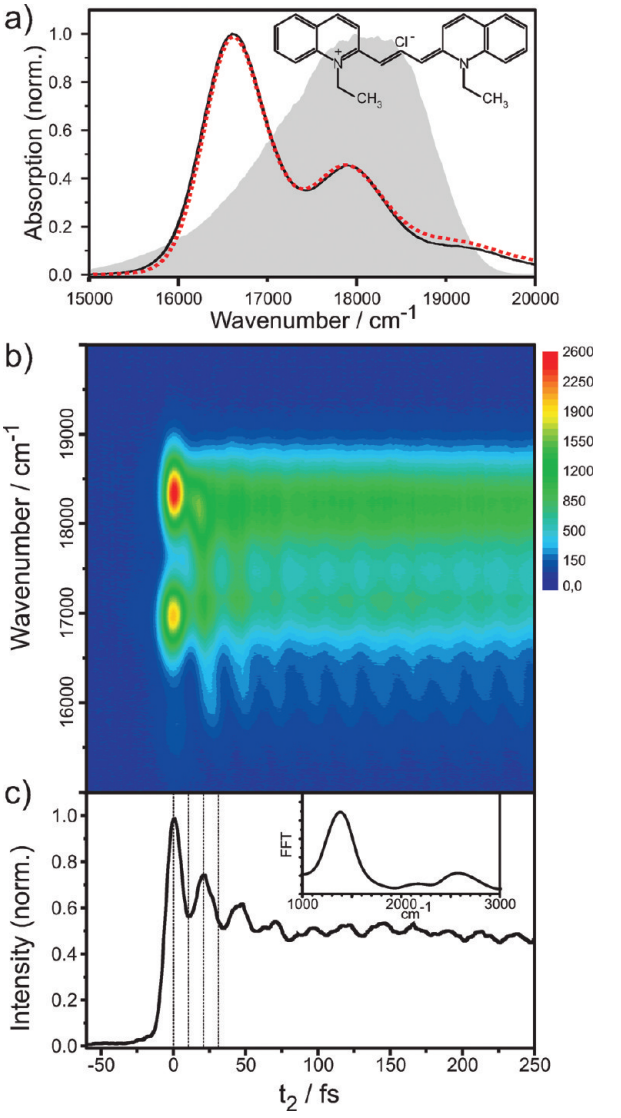

Figure 3. (a) Experimental (black solid line) and simulated (red dashed line) absorption spectrum of Pinacyanol chloride (PIN) and comparison to the laser pulse spectrum (gray shaded area). The chemical structure of PIN is shown as an inset. (b) Frequency resolved and (c) frequency integrated transient grating (TG) data. The grid lines indicate t_2 = 0, 10, 20, and 30 fs. The inset shows the power spectrum of the Fourier transform of the TG data.

nonrephasing response functions.[22] We can thus write

$$S^{(3)}(t_1, t_2, t_3) = R_{NR}(t_1, t_2, t_3) + R_R(t_1, t_2, t_3) \quad (2)$$

with

$$R_{NR}(t_1, t_2, t_3) = R_1(t_1, t_2, t_3) + R_4(t_1, t_2, t_3) \quad (3)$$

and

$$R_R(t_1, t_2, t_3) = R_2(t_1, t_2, t_3) + R_3(t_1, t_2, t_3) \quad (4)$$

The response functions contributing to the signal depends on the order of interaction of the electric fields with the wave-vectors $-\mathbf{k_1}$, $\mathbf{k_2}$, and $\mathbf{k_3}$. For an interaction order 1−2−3 (2−1−3), the signal reflects the rephasing (nonrephasing) response functions. For finite pulses, one must average over all possible orderings and actual time delays between the electric field interaction permitted

dx.doi.org/10.1021/jp109442b |J. Phys. Chem. B 2011, 115, 5383–5391

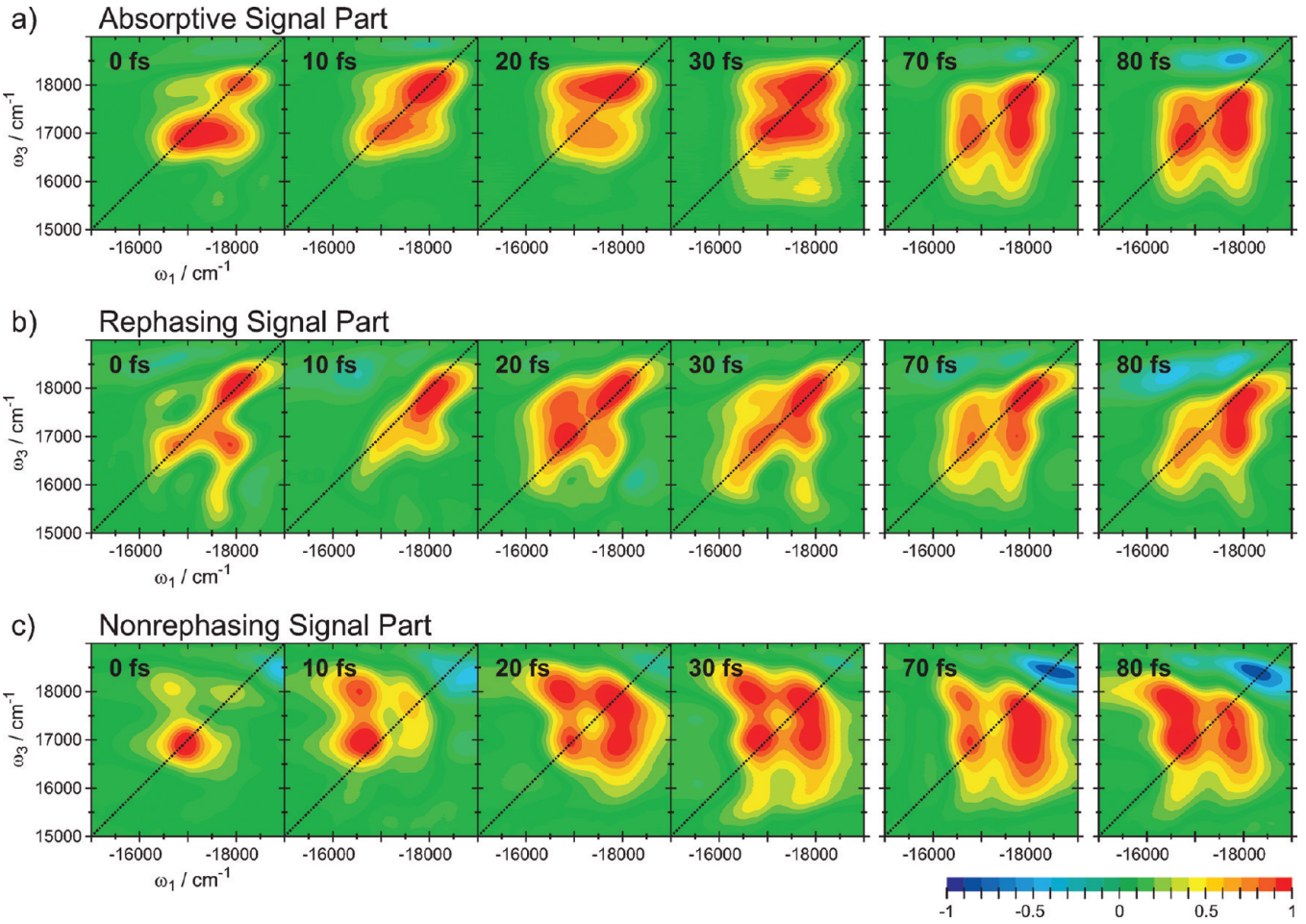

Figure 4. Experimental (a) real part of the total 2D spectrum with (b) rephasing and (c) nonrephasing contributions. The waiting times t_2 are indicated in each figure. All spectra are normalized to their respective maximum.

by the finite envelopes.[34,38] For the simulations of the 2D spectra below we employ the electric fields extracted from independently measured SHG-FROG experiments shown in Figure 2[29] and follow the treatment given in ref 38. Having calculated the nonlinear polarization, the 2D spectrum is generated by a double Fourier transform.[34]

The response functions represent the central quantity in the simulations of the nonlinear spectra. By using the second order cumulant expansion,[22] we can express these response functions via the line shape function $g(t)$. The result for the two-level system can be found in the literature.[22,39,40] Making use of the temperature independent spectral density $(C(\omega))$, we can write the line shape functions as

$$g(t) = \frac{1}{2\pi}\int_{-\infty}^{\infty} d\omega\ (1-\cos(\omega t))\coth(\beta\hbar\omega/2)\frac{C(\omega)}{\omega^2} + \frac{i}{2\pi}\int_{-\infty}^{\infty} d\omega\ (\sin(\omega t)-\omega t)\frac{C(\omega)}{\omega^2} \quad (5)$$

where β is the inverse temperature. The spectral density describes the spectrum of the modes modulating the transition frequency weighted by the strength of each component, and it can have a number of different contributions including solvent modes and underdamped vibrations of the solute.[41] From the line shape function, we can directly calculate the shape of the linear absorption as the real part of the one sided Fourier transform of $\exp(-g(t))$.[22] The model employed in this work is commonly referred to as the Brownian oscillator model, which together with the cumulant expansion accounts for correlation of bath fluctuations during different time periods, satisfies the fluctuation−dissipation relation, and is capable of describing the development of the Stokes shift.[22]

For the present model, the spectral density determines the shape of the linear spectra as well as the shape of the 2D spectrum and its time evolution. In this work we adopt a minimal model of the spectral density capable of reproducing the oscillations observed in the 2D spectrum. We find that at least one vibrational mode is required to describe the vibrational progression in the linear absorption spectrum shown in Figure 3a. We model this via an underdamped mode[22] with a frequency of 1310 cm^{-1} and a reorganization energy of 630 cm^{-1}. By repeated calculations of the linear and nonlinear spectra, we find that at least two overdamped nuclear modes are necessary in addition to the vibrational mode in order to reach satisfactory agreement with the experiments. We model these two overdamped modes as having an exponential time dependence,[42] with characteristic times of 20 and 100 fs and reorganization energies of 150 and 225 cm^{-1} respectively.

RESULTS AND DISCUSSION

Coherent Regime. The experimental results are shown in Figure 4, whereas the simulations, based on the model discussed

dx.doi.org/10.1021/jp109442b |J. Phys. Chem. B 2011, 115, 5383–5391

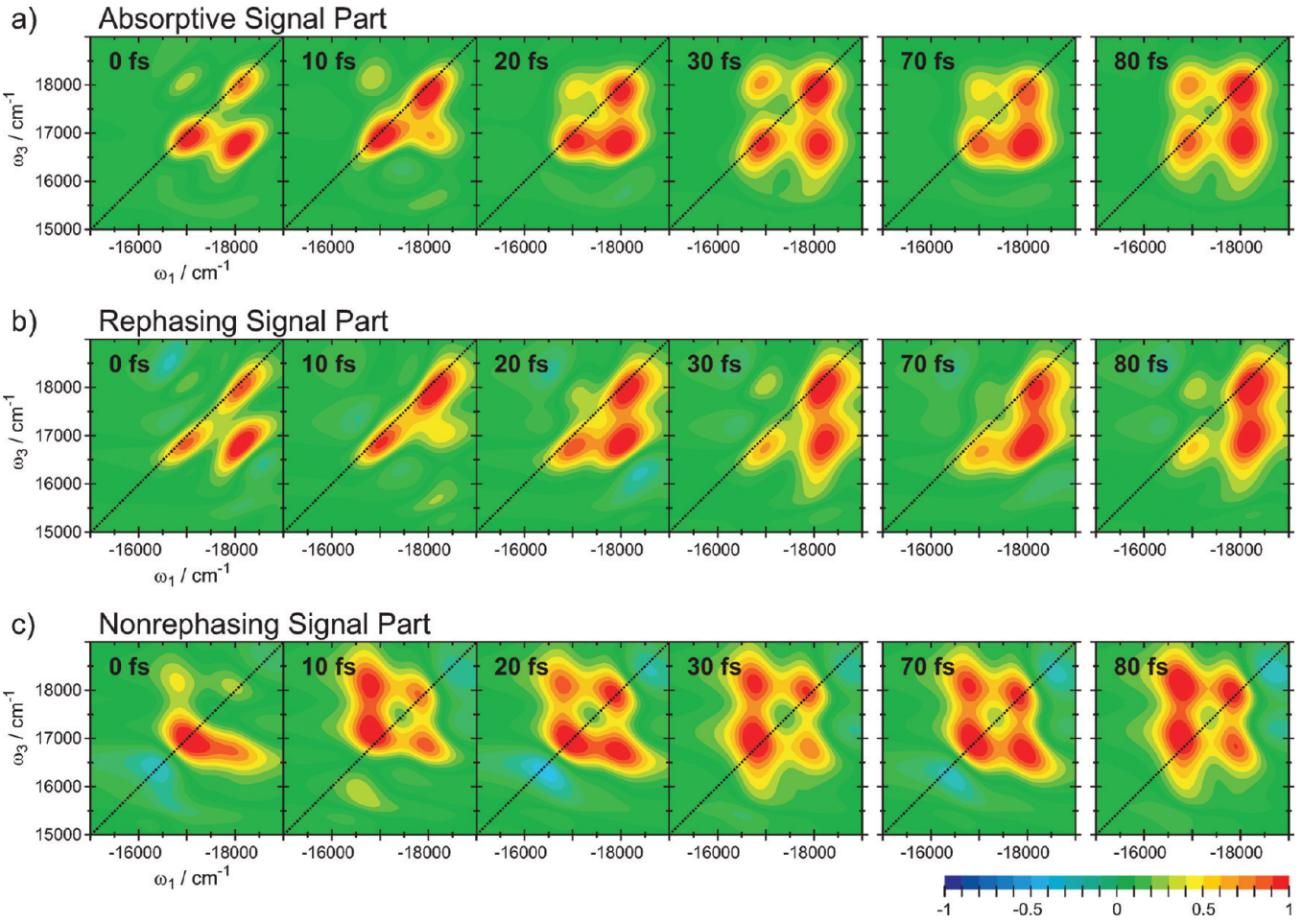

Figure 5. Simulation of the 2D spectrum with the model discussed in the text. (a) Real part of the total 2D spectrum with (b) rephasing and (c) nonrephasing contributions. The waiting times t_2 are indicated in each spectrum. All spectra are normalized to their respective maximum.

in the previous section, are shown in Figure 5. The total 2D correlation spectrum ($t_2 = 0$ fs, Figure 4a) is characterized by two diagonal- and two off-diagonal peaks. The lower diagonal peak is located at $\omega_1 = \omega_3 = \omega_0$, where ω_0 is the frequency of the electronic system in the absence of coupling to vibrational modes. The higher peak includes one vibrational quantum and is located at $\omega_1 = \omega_3 = \omega_0 + \nu_{vib}$, where ν_{vib} is the frequency of the underdamped vibrational mode (1300 cm^{-1}) responsible for the high energy peak in the linear absorption spectrum. Additionally we find two weak off-diagonal peaks both above and below the diagonal. These off-diagonal peaks are much more resolved in the rephasing (R) and nonrephasing (NR) spectra than in the total absorptive spectrum. The R spectrum emphasizes the features related to the vibrational mode, i.e. the upper diagonal peak as well as the two off-diagonal peaks, while the NR spectrum is dominated by the lower diagonal peak. In addition to the four peak pattern, we observe a weak off-diagonal peak at ($\omega_1 = 17\,750$ cm^{-1}, $\omega_3 = 15\,750$ cm^{-1}). This peak has contributions in the R pulse order only, and can be traced to the Feynman diagrams in Figure 6a. These two diagrams can propagate in either excited or ground state vibrational coherence during t_2 and are both of R type. Both diagrams involve a vibrational coherence in the ground state after the third interaction, and it is not possible to construct the corresponding diagram for the NR pulse order.

The evolution ($t_2 > 0$) of the 2D spectrum shown in Figure 4 can be divided into two phases. The first phase represents coherent evolution and lasts up to $t_2 = 30$ fs. The coherent phase represents reversible dynamics prior to the onset of relaxation and is characterized by a temporal change of the amplitude and position of the diagonal- and off-diagonal peaks. Going from $t_2 =$ 0 to 10 fs, we find that the off-diagonal peaks lose intensity, and all four peaks move toward the center of the spectrum. The delay of 10 fs corresponds to a minimum of the TG signal (Figure 3c), and we can conclude that the overall amplitude of the diagonal peak has decreased. At the same time the high energy diagonal peak gains intensity compared to the lower one. This increased intensity then remains throughout the t_2 series. The same feature is present in the simulations, and therefore not related to the presence of excited state absorption (ESA) neglected in the model (see below). The evolution of the total 2D spectrum is rather modest compared to the changes in the R and NR spectra. Interestingly, the R (NR) spectra emphasize the lower (upper) off-diagonal peak and this feature is nicely reproduced in the simulations. The R spectra show similar features as the total spectrum. Going from $t_2 = 0$ to 10 fs, we find that the off-diagonal peaks lose intensity and become elongated along the antidiagonal. Contrary to the oscillatory motions of the off-diagonal peaks in the R spectra, the NR spectra show no such features. Starting from $t_2 = 0$ fs, where the lower diagonal peak dominates the

dx.doi.org/10.1021/jp109442b |J. Phys. Chem. B 2011, 115, 5383–5391

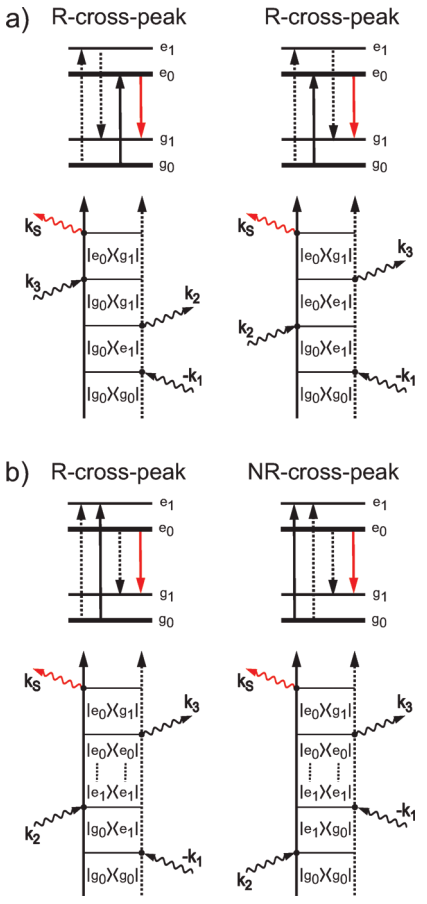

Figure 6. (a) Rephasing Feynman diagrams contributing to the off-diagonal peak at ω_1 = 17 750 cm^{-1} and ω_3 = 15750 cm^{-1} in the correlation spectrum (Figure 4a). The left (right) diagram evolves in the ground (excited) state during t_2. Both diagrams involve the interaction with the vibrational mode in the ground state during t_3. It is not possible to construct a nonrephasing analogue to these diagrams that would give signal at these same frequencies. (b) Feynman diagrams illustrating the contributions to the ω_1 = 17 750 cm^{-1} and ω_3 = 15 750 cm^{-1} off-diagonal peak after relaxation in the excited state.

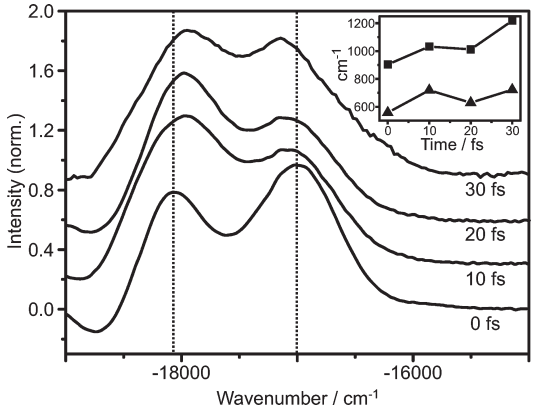

Figure 7. Diagonal slices of the real part of the 2D spectrum for t_2 = 0, 10, 20, and 30 fs corresponding to in-phase (0 and 20 fs) and out of phase (10 and 30 fs) positions of the wavepacket. The dashed lines mark the two peak maxima at t_2 = 0 fs. The insert shows the fwhm in cm^{-1} of the two peaks as obtained from a fit to two Gaussians where the square (triangle) denotes the low (high) energy peak.

spectrum, the NR spectrum develops the characteristic four-peak pattern after 20 fs. The lower diagonal peak loses intensity to the higher diagonal peak as well as to the off-diagonal ones. The elongation of the off-diagonal peaks along the antidiagonal for t_2 = 10 fs in the total 2D spectrum can be understood from the lack of signal in the R spectrum. For this delay the signal is dominated by the NR component which is, as expected, elongated along the antidiagonal.[4,6,43]

For a more detailed view of the changes of the 2D spectrum due to the modulation by the coherences, we plot in Figure 7 the diagonal slice for t_2 = 0, 10, 20, and 30 fs. As can be seen from the transient grating signal in Figure 3c, these times represent in-phase (0 and 20 fs) and out-of-phase (10 and 30 fs) contributions. The diagonal slices give a more detailed view on the influence of the oscillatory motion on the 2D spectrum. We find that the diagonal peaks move closer together for out of phase delays, and that this effect is more pronounced for the high frequency peak. At the same time there are changes in the width of the peaks. To extract the diagonal width we used a double Gaussian function to fit the two peaks. The resulting fwhm is shown in the insert for the different delays. As can be seen, the diagonal width oscillates as the system goes through the oscillation, where the broader diagonal width is observed when the amplitude is low. For the low energy peak the width increases with time and there is only a weak indication of an oscillation.

We ascribe this broadening to relaxation and development of the Stokes shift as will be discussed below. The simulations shown in Figure 5 reproduce the main features of the oscillations in the diagonal peaks seen in the experiments (Figures 4 and 7).

We repeated the simulations to ensure that the observation is not specific to this experiment (i.e., pulse chirp, finite bandwidth) or due to overlapping signal contributions (ESA). Figure 8 shows model calculations where the electronic transitions to the overdamped modes is decreased by a factor of 2. For these calculations, we employ 6 fs transform limited pulses. The simulations shown in Figure 8 display the characteristics of the experiments and simulations, i.e., the decreased frequency splitting between the peaks as well as an increased peak broadening as the amplitude of the peaks goes down. The modulation of the 2D spectra reported in this contribution differ from previous reports of wavepacket modulation in a PERY[44] dye.[4,6] In these works it was found that the modulation of the amplitude and width was correlated and these results were successfully analyzed with a model[4,43] similar to the one used here. This difference could in principle be explained by a number of effects. For instance, the bath correlation time is shorter than the oscillatory period in PERY, whereas the opposite is true for PIN. Furthermore, due to the low frequency of the vibrational mode, all diagonal and off-diagonal peaks overlap in the spectrum of PERY. However, when repeating the simulations with the new parameters we find that none of these effects can explain the observed differences. We find that the center frequency of the laser is the decisive factor for the observation of correlation or anticorrelation between the width and the amplitude modulation. If probing on the red edge (like in PERY[4]), we find correlation, whereas exciting close to the center of the spectrum (PIN) gives rise to an anticorrelation. This dependence of wavepacket signatures on the experimental parameters calls for caution in extrapolation of experimental results obtained under different experimental conditions.

Experiments and simulations show that the center frequency of the peaks change as the system goes through an oscillation. The change in frequency of the peaks along ω_3 would, in pump−probe

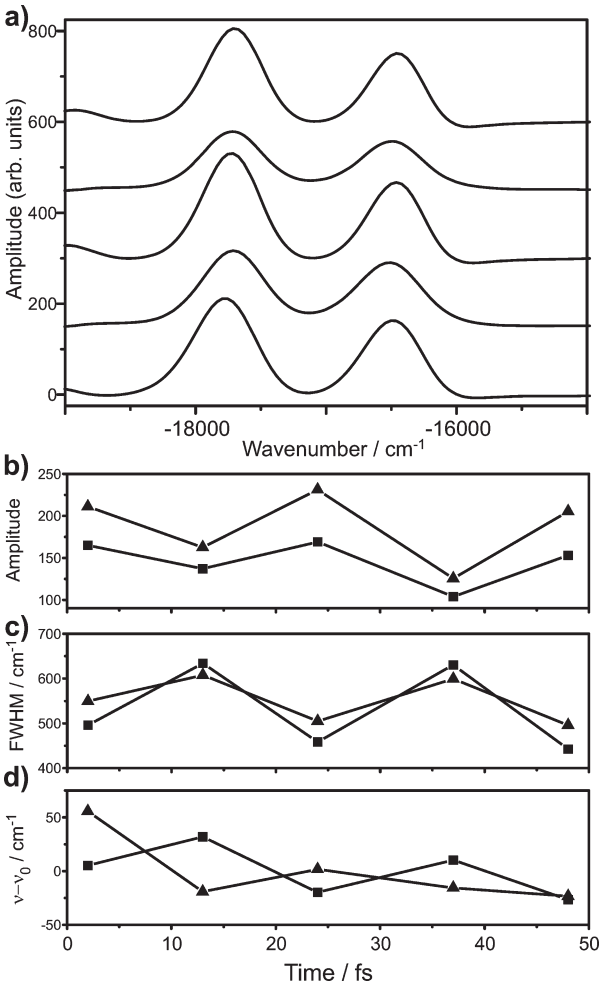

Figure 8. (a) Diagonal slices of the 2D spectra for the PIN model with weaker coupling to overdamped modes for t_2 = 2, 13, 24, 37, and 48 fs, corresponding to maxima (2, 24, and 48 fs) and minima (13 and 37 fs) of the transient grating signal. The slices for different t_2 are not normalized. A fit with two Gaussians visualizes the oscillations in the (b) amplitude, (c) width of each peak, and (d) center frequency, where the squares (triangles) denote the low (high) energy peak. The mean frequency of each peak in (d) was subtracted to visualize the anticorrelation in the frequency shift of the two peaks.

language, correspond to different positions of the wavepacket in the potential as a function of t_2.

At the outer turning point, the energy difference between the potential energy surfaces is lower, and one would observe a redshift of the signal. We point out that such effects require the correlation of nuclear motions during different time periods and cannot be properly described in the homogeneous limit (one must keep track of the position of the wave packet in the potential). We conclude that the concerted change in the peak position along ω_1 and ω_3 requires correlation of bath motions during the different time periods. In the pump−probe picture, one usually thinks of a wavepacket without any previous history (i.e., independent of ω_1) which then propagates in the potential and gives rise to a time dependent transition frequency in ω_3. In practice one does not generate a wavepacket that is independent of the history of the first coherence period. We stress that if the system is in a coherent state, one must be careful in interpreting the ω_1 and ω_3 dynamics as "absorption" and "emission", and that this interpretation is only applicable for times longer than the bath correlation time (or in the homogeneous limit). Such a view of the t_2 dependence of the spectrum in the coherent phase leads to unphysical conclusions about the dynamics of the wavepacket. However, a model properly including the correlated bath motions during the different time periods readily reproduces this unintuitive behavior of wavepackets in the 2D spectrum.

The oscillatory pattern induced by the high frequency underdamped mode is very rich and leads to complicated dynamics of both diagonal and off-diagonal peaks. In this work we focus on the oscillations of the diagonal peak in order to compare to the results in ref 26. However, it is clear that the off-diagonal peaks also oscillate. A detailed analysis of the modulation of the 2D spectrum by a high frequency mode[43] revealed that the oscillatory behavior was different for the off-diagonal peaks as compared to the diagonal ones. We observe a similar behavior in our model. The different oscillations of the diagonal and off-diagonal peaks were traced to the mixing in of the imaginary component of the response function for the off-diagonal peaks.[43] For a well resolved vibrational progression, this mixing leads to the appearance of time dependent negative features associated with the vibrational off-diagonal peaks.

Irreversible Regime. The coherent phase of the evolution of the 2D spectrum is remarkably short and already at t_2 = 30 fs we see clear signatures of irreversible dynamics. During this phase the vibrational modulation of the spectrum continues, but is now accompanied by relaxation and the formation of a red-shifted stimulated emission (SE) signal. The 2D spectrum attains a square shape already after 30−40 fs (Figure 4) and is accompanied by the increased symmetry of the individual peaks. In addition, the off-diagonal peaks become more resolved and symmetric for longer waiting times. As a result of relaxation, the new diagonal and off-diagonal peaks below $\omega_3 = 16\,000$ cm^{-1} acquire significant amplitudes. In order to match the rise of these components in the simulations, we need to use a very fast component in the correlation function (20 fs).

The downward motion of the spectrum and the elongation of the peaks leads to a change in the appearance of the off-diagonal peaks in R and NR signals. The off-diagonal peak at (ω_1 = 17 750 cm^{-1} and ω_3 = 15 750 cm^{-1}) observed at t_2 = 0 fs only shows contributions in the R spectrum (Figure 4b). At longer t_2 times, the fast relaxation leads to a streaking along ω_3 and the appearance of the signal at (ω_1 = 17 750 cm^{-1} and ω_3 = 15 750 cm^{-1}). However, at t_2 = 70 fs we find that both NR and R contribute to this feature. This reflects the relaxation and the build up of the Stokes shift. We illustrate this by the Feynamn diagrams in Figure 6b. Including relaxation from a populated nuclear mode in the excited state during t_2, we can construct the corresponding R and NR diagrams and account for our observations.

The complex relaxation dynamics of the positive features of the 2D spectrum is accompanied by a weak negative signal at $\omega_3 > 18\,500$ cm^{-1}. In accordance to previous pump−probe experiments,[45] we ascribe this to ESA from the first excited state. This signal is significantly blue-shifted from the SE and GSB. As such, the interference between GSB/SE and ESA would mostly affect the upper peak. Despite this we see a similar modulation of both the upper and the lower peak (cf. Figure 7). Therefore we conclude that the modulation of the GSB/SE peaks are only weakly affected by the presence of ESA in the coherent regime. For this reason we neglected the pathways involving the ESA

transitions in the modeling of the 2D spectra where we focused on the oscillations.

The development of the Stokes shift leads to a redistribution of strength from the upper line of peaks to the lower ones in the spectrum. We note that our model cannot fully account for the appearance of the signal at longer times (t_2 > 70 fs) and underestimates the redistribution of signal strength in the spectrum. With the excited state relaxed (t_2 > 70 fs), we should still observe the high energy peaks due to GSB at longer times. From Figure 4 it is clear that these GSB peaks are distorted due the ESA signal at high ω_3 energy. This indicates that the ESA in this spectral region becomes stronger as the system relaxes in the excited state. This ESA contribution should be included for a quantitative agreement between simulations and experiments in the irreversible regime, but is beyond the scope of the present work.

CONCLUSIONS

The peak pattern and the oscillatory motions observed in the coherent phase show similarities to the results obtained for a dimer model system by Pisliakov et al.[26] In addition to amplitude modulations of the off-diagonal peaks, the authors also observed a modulation of the diagonal peaks. It was found that the diagonal width of the diagonal peaks increased as the overall amplitude of the peaks decreased. This anticorrelation of the diagonal width and the amplitude was later used by a number of groups to argue that this type of modulation represents electronic coherence dynamics.[16,18]

Our experimental results show that such anticorrelated motion can be observed even for nuclear wavepackets and is captured in a theory including only vibrational coherences. Therefore, the previously assumed connection between this type of modulation of the 2D spectra and exciton motion is not unique. In fact, considering the Feynman diagrams for a dimer and a TLS coupled to a single vibrational mode, we conclude that most of the signal contributions are the same for these models (Figure 1). To assign the oscillation to a specific coherence one must identify pathways that are unique to each model (i.e., electronic or nuclear). In the case of the dimer this could be achieved by identification of the pathways involving the doubly excited state f. However, even molecules may have ESA in the spectral region of GSB,[32,46] which makes such assignments difficult in practice. For nuclear coherences, the unique pathways involve the ground state vibrational level. This type of contribution has been observed previously with strongly red-shifted excitation in β-carotene[47] and is also observed here (the low ω_3 off-diagonal peak in Figure 4a and the Feynman diagram in Figure 6a). However, such observations will be difficult to distinguish if the frequency of the oscillation is lower and the linear absorption spectrum does not exhibit resolved peaks.

In addition to the oscillations of the off-diagonal peaks, their shape has been used to determine the correlation between the two exciton states.[14] In light of the time dependent contributions from R and NR pathways, the shape of the cross-peaks also depends on t_2 and such arguments should be applied to the correlation spectrum only.

Our observations show that one typically needs auxiliary information in order to assign oscillatory motion in the 2D spectrum to electronic coherences. In special cases one can extract the exciton beat frequency directly from the linear absorption spectrum.[14] In protein-pigment complexes, knowing the structure is essential in order to determine the correspondence between the observed frequencies and the beat frequency between the exciton levels.[16] If the structure is not known, it is more difficult to estimate the exciton splitting since the linear absorption spectrum of protein-pigment complexes is usually inhomogenously broadened and does not show well resolved peaks even at low temperature.[48] In these cases the frequencies and coupling strengths of the vibrational modes should be probed by an additional measurement, for instance resonance Raman[49] or fluorescence line narrowing.[50,51] Alternatively one can employ different polarizations of the laser fields to decide the nature of the oscillating components[14] in the 2D spectrum.

We conclude that high frequency vibrational motions can significantly change the appearance of the 2D spectrum as they give rise to additional diagonal and off-diagonal peaks. These peaks move and change shape as a function of the waiting time and make the interpretation of the 2D spectra more complicated. Because the modulations of the diagonal (and off-diagonal) peaks are a direct consequence of the presence of a high frequency mode in the correlation function (in the electronic two-level model and the interference of many different contributions),[43] it is difficult to provide a simple and intuitive explanation for the observed modulations.

We find that the t_2 dependence can be divided into two separate phases, one representing coherent motion and one where relaxation has set in. In the latter phase, relaxation leads to the formation of SE causing a streaking of the 2D spectrum along the ω_3 direction and reshaping of the amplitude of the off-diagonal peaks. In the coherent phase we find clear changes in both the peak positions and the widths of the diagonal peaks as the system oscillates. The oscillations of the diagonal peaks display an anticorrelation between the diagonal width and the amplitude. This type of modulation has previously been associated with electronic coherences but can, as we have shown here, also result from vibrational coherences. We thus conclude that neither the observation of off-diagonal peaks nor anticorrelated width and amplitude modulation can be taken as a unique proof of electronic coherences.

AUTHOR INFORMATION

Corresponding Author
*E-mail: harald.f.kauffmann@univie.ac.at.

ACKNOWLEDGMENT

This work was supported by the Austrian Science Foundation (FWF) within the Projects P223311 and F016−18 (SFB ADLIS). A.N. appreciates the support by the Austrian Academy of Sciences (ÖAW) through a DOC-fforte scholarship. N.C. acknowledges support from the Wenner-Gren foundation. F.M. acknowledges support by the Deutsche Forschungsgemeinschaft through the DFG-Cluster of Excellence Munich-Centre for Advanced Photonics.

REFERENCES

(1) Schrödinger, E. *Naturwissenschaften* **1926**, *14*, 664.
(2) Fragnito, H. L.; Bigot, J.-Y.; Becker, P. C.; Shank, C. V. *Chem. Phys. Lett.* **1989**, *160*, 101–104.
(3) Ohta, K.; Larsen, D. S.; Yang, M.; Fleming, G. R. *J. Chem. Phys.* **2001**, *114*, 8020–8039.

(4) Nemeth, A.; Milota, F.; Mančal, T.; Lukeš, V.; Kauffmann, H. F.; Sperling, J. *Chem. Phys. Lett.* **2008**, *459*, 94–99.
(5) Tekavec, P. F.; Myers, J. A.; Lewis, K. L. M.; Ogilvie, J. P. *Opt. Lett.* **2009**, *34*, 1390–1392.
(6) Nemeth, A.; Milota, F.; Mančal, T.; Lukes, V.; Hauer, J.; Kauffmann, H. F.; Sperling, J. *J. Chem. Phys.* **2010**, *132*, 184514–1 − 184514−11.
(7) Wang, Y.; Kobayashi, T. *ChemPhysChem* **2010**, *11*, 889–896.
(8) May, V.; Kühn, O. *Charge and energy Transfer Dynamics in Molecular Systems*; Wiley/VCH: Berlin, 1999.
(9) Chachisvilis, M.; Kuhn, O.; Pullerits, T.; Sundström, V. *J. Phys. Chem. B* **1997**, *101*, 7275–7283.
(10) Brixner, T.; Stenger, J.; Vaswani, H. M.; Cho, M.; Blankenship, R. E.; Fleming, G. R. *Nature* **2005**, *434*, 625–628.
(11) Cheng, Y. C.; Silbey, R. J. *Phys. Rev. Lett.* **2006**, *96*, 028103.
(12) Ishizaki, A.; Calhoun, T. R.; Schlau-Cohen, G. S.; Fleming, G. R. *Phys. Chem. Chem. Phys.* **2010**, *12*, 7319–7337.
(13) Milota, F.; Sperling, J.; Nemeth, A.; Abramavicius, D.; Mukamel, S.; Kauffmann, H. F. *J. Chem. Phys.* **2009**, *131*, 054510–1 − 054510−23.
(14) Womick, J. M.; Miller, S. A.; Moran, A. M. *J. Phys. Chem. B* **2009**, *113*, 6630–6639.
(15) Panitchayangkoon, G.; Hayes, D.; Fransted, K. A.; Caram, J. R.; Harel, E.; Wen, J.; Blankenship, R. E.; Engel, G. S. *Proc. Natl. Acad. Sci. U.S.A.* **2010**, *107*, 12766–12770.
(16) Engel, G. S.; Calhoun, T. R.; Read, E. L.; Ahn, T.-K.; Mančal, T.; Cheng, Y.-C.; Blankenship, R. E.; Fleming, G. R. *Nature* **2007**, *446*, 782–786.
(17) Calhoun, T. R.; Ginsberg, N. S.; Schlau-Cohen, G. S.; Cheng, Y.-C.; Ballottari, M.; Bassi, R.; Fleming, G. R. *J. Phys. Chem. B* **2009**, *113*, 16291–16295.
(18) Collini, E.; Scholes, G. D. *Science* **2009**, *323*, 369–373.
(19) Collini, E.; Wong, C. Y.; Wilk, K. E.; Curmi, P. M. G.; Brumer, P.; Scholes, G. D. *Nature* **2010**, *463*, 644–647.
(20) Wells, N. P.; Blank, D. A. *Phys. Rev. Lett.* **2008**, *100*, 086403−1–086403−4.
(21) Egorova, D. *Chem. Phys.* **2008**, *347*, 166–176.
(22) Mukamel, S. *Principles of Nonlinear Optical Spectroscopy*; Oxford University Press: Oxford, 1995.
(23) Jonas, D. M. *Annu. Rev. Phys. Chem.* **2003**, *54*, 425–463.
(24) Cho, M. H. *Chem. Rev.* **2008**, *108*, 1331–1418.
(25) Egorova, D.; Gelin, M. F.; Domcke, W. *J. Chem. Phys.* **2007**, *126*, 074314−1–074314−11.
(26) Pisliakov, A. V.; Mančal, T.; Fleming, G. R. *J. Chem. Phys.* **2006**, *124*, 234505−1–234505−14.
(27) Piel, J.; Riedle, E.; Gundlach, L.; Ernstorfer, R.; Eichberger, R. *Opt. Lett.* **2006**, *31*, 1289–1291.
(28) Baum, P.; Breuer, M.; Riedle, E.; Steinmeyer, G. *Opt. Lett.* **2006**, *31*, 2220–2222.
(29) Trebino, R. *Frequency-Resolved Optical Gating: The Measurement of Ultrashort Laser Pulses*; Kluwer Academic Publishers: Boston, 2002.
(30) Khalil, M.; Demirdöven, N.; Tokmakoff, A. *Phys. Rev. Lett.* **2003**, *90*, 47401.
(31) Nemeth, A.; Sperling, J.; Hauer, J.; Kauffmann, H. F.; Milota, F. *Opt. Lett.* **2009**, *34*, 3301–3303.
(32) Nemeth, A.; Milota, F.; Mančal, T.; Pullerits, T.; Sperling, J.; Hauer, J.; Kauffmann, H. F.; Christensson, N. *J. Chem. Phys.* **2010**, *133*, 094505−1–094505−15.
(33) Gundogdu, K.; Stone, K. W.; Turner, D. B.; Nelson, K. A. *Chem. Phys.* **2007**, *341*, 89–94.
(34) Brixner, T.; Mančal, T.; Stiopkin, I. V.; Fleming, G. R. *J. Chem. Phys.* **2004**, *121*, 4221–4236.
(35) Nemeth, A.; Lukeš, V.; Sperling, J.; Milota, F.; Kauffmann, H. F.; Mančal, T. *Phys. Chem. Chem. Phys.* **2009**, *11*, 5986–5997.
(36) Tauber, M. J.; Mathies, R. A.; Chen, X.; Bradforth, S. E. *Rev. Sci. Instrum.* **2003**, *74*, 4958–4960.
(37) Laimgruber, S.; Schachenmayr, H.; Schmidt, B.; Zinth, W.; Gilch, P. *Appl. Phys. B: Laser Opt.* **2006**, *85*, 557–564.
(38) Christensson, N.; Avlasevich, Y.; Yartsev, A.; Müllen, K.; Pascher, T.; Pullerits, T. *J. Chem. Phys.* **2010**, *132*, 0174508−1–174508−10.
(39) Cho, M.; Yu, J.-Y.; Joo, T.; Nagasawa, Y.; Passino, S. A.; Fleming, G. R. *J. Phys. Chem.* **1996**, *100*, 11944–11953.
(40) Cho, M. H. *Two-dimensional optical spectroscopy*; CRC Press: Boca Raton, FL, 2009.
(41) Christensson, N.; Dietzek, B.; Yartsev, A.; Pullerits, T. *Chem. Phys.* **2009**, *357*, 85–95.
(42) Yang, M.; Ohta, K.; Fleming, G. R. *J. Chem. Phys.* **1999**, *110*, 10243–10252.
(43) Mančal, T.; Nemeth, A.; Milota, F.; Lukes, V.; Kauffmann, H. F.; Sperling, J. *J. Chem. Phys.* **2010**, *132*, 184515−1–184515−12.
(44) *N,N′*-Bis(2,6-dimethylphenyl)perylene-3,4,9,10-tetracarboxylicdiimide.
(45) Meyer, Y. H.; Pittman, M.; Plaza, P. *J. Photochem. Photobiol. A: Chem.* **1998**, *114*, 1–21.
(46) Christensson, N.; Milota, F.; Nemeth, A.; Pugliesi, I.; Riedle, E.; Sperling, J.; Pullerits, T.; Kauffmann, H. F.; Hauer, J. *J. Phys. Chem. Lett.* **2010**, *1*, 3366–3370.
(47) Christensson, N.; Milota, F.; Nemeth, A.; Sperling, J.; Kauffmann, H. F.; Pullerits, T.; Hauer, J. *J. Phys. Chem. B* **2009**, *113*, 16409–16419.
(48) Peterman, E. J. G.; Pullerits, T.; van Grondelle, R.; van Amerongen, H. *J. Phys. Chem. B* **1997**, *101*, 4448–4457.
(49) Lawless, M. K.; Mathies, R. A. *J. Chem. Phys.* **1992**, *97*, 8037–8045.
(50) Christensson, N.; Dietzek, B.; Yartsev, A.; Pullerits, T. *Vib. Spec.* **2010**, *53*, 2–5.
(51) Pullerits, T.; Monshouwer, R.; van Mourik, F.; van Grondelle, R. *Chem. Phys.* **1995**, *194*, 395–407.